Letter

Broken symmetry and competing orders in Weyl semimetal interfaces

Ritajit Kundu,[1] H. A. Fertig,[2,3] and Arijit Kundu[1]
[1]*Department of Physics, Indian Institute of Technology Kanpur, Kanpur 208016, India*
[2]*Department of Physics, Indiana University, Bloomington, Indiana 47405, USA*
[3]*Quantum Science and Engineering Center, Indiana University, Bloomington, Indiana 47408, USA*

(Received 23 April 2022; revised 20 November 2022; accepted 19 December 2022; published 9 January 2023)

We consider interaction-induced broken symmetry states of two Weyl semimetal surfaces with multiple Fermi-arc (FA) states. In the presence of inter- and intrasurface Coulomb interactions, multiple broken symmetries may emerge which coexist and/or compete with one another. Interlayer exciton condensates involving different FA flavors are shown to form, with amplitudes determined by the strength of interactions and the degree of nesting among the arcs. For FA pairs which are well separated in momentum with strong nesting, the resulting state is a particle-hole analog of a Fulde-Ferrell-Larkin-Ovchinnikov (FFLO) superconductor. Intralayer interactions moreover induce charge density wave (CDW) ordering, so that the most general state of the system is a supersolid. These orderings in principle carry signatures in nonlinear behavior and narrow band noise in Coulomb drag transport measurements.

DOI: 10.1103/PhysRevB.107.L041402

I. INTRODUCTION

Weyl semimetals (WSMs) are three-dimensional topological systems with an even number of band-touching points (Weyl nodes) in their bulk band structure [1,2]. Because of their intrinsic topology, nonoverlapping surface projections of Weyl nodes connect endpoints of disjoint Fermi surface sections known as Fermi arcs (FAs). FAs host surface states that disperse in a quasi-one-dimensional manner. There are extensive ongoing efforts to identify material candidates for WSMs, both theoretically and experimentally. Examples of such materials include TaAs [3], NbAs [4], and, more recently, CoSi, $Co_3Sn_2S_2$, for which FA modes have been identified in angle-resolved photoemission spectroscopy (ARPES) and quasiparticle interference experiments [5–7]. Although they may lack topological protections, FAs of Dirac semimetals, such as Na_3Bi and Cd_3As_2, have also been identified in recent times [8–13].

Interactions may introduce interesting physics in WSMs, involving either or both the bulk states and the FA states. For example, collective excitations confined to the surfaces are expected to be supported [14–23], as are bulk excitonic modes and density-wave instabilities [24,25], among other possibilities [2]. Interesting effects also occur when two Weyl systems are brought together. For example, intricate reconstruction of FA geometry can sometimes occur due to intersurface tunneling [26–28]. In the absence of tunneling, intersurface Coulomb interactions may induce coherent particle-hole processes involving FA states of both surfaces, leading to new collective excitations and broken symmetry states. This is the subject of our study. As explained below, we find that a number of symmetries may break in such systems: the local gauge symmetry, which conserves the particle number of each layer, due to intersurface exciton condensation [29], in similarity with other bilayer systems, such as in graphene [30–32]; translational symmetry, through the formation of charge-density-wave (CDW) order; and, in each case, coherences may set in among different pairs of arcs on the same or different surfaces, yielding multiple ways in which these kinds of orders set in. As we shall see, while these orderings coexist, they also compete, leading to quantum phase transitions among different realizations of the broken symmetries with variations of the system parameters.

Associated with these broken symmetry states are Goldstone modes. The broken translational symmetry characteristic of CDW order leads to phonon modes, which at zero wave vector becomes a sliding mode that is generically pinned by disorder [33]. Exciton condensation yields gapless superfluid modes [34–37], which in such double-layer systems are realized as a dissipationless counterflow current. Moreover, very weak tunneling between surfaces may yield Josephson-like transport behavior between them [38,39]. Such collective behavior can be observed in a variety of transport experiments [39–43].

As a paradigm of such systems, we consider a setup of two capacitively coupled WSM surfaces, each hosting FAs (see Fig. 1). For simplicity we consider straight arcs, although our qualitative results do not depend significantly on this simplification (see Supplemental Material (SM) [44]). We find that electron-hole coherence may develop among some or all of the arcs, depending on their relative angles and interaction strengths. For arcs on different surfaces with common in-plane wave vectors, strong interlayer coherence can develop at these common wave vectors [29]. Interlayer coherence can also develop between arcs on different surfaces whose wave vectors are remote from one another, and surprisingly, these coherences can be stronger than the direct case, particularly when the arcs are nested. Such finite momentum interlayer ordering may be understood as an exciton condensate analog of the Fulde-Ferrell-Larkin-Ovchinikov (FFLO) superconductor. We find that these direct exciton (D-ex) and FFLO exciton (FFLO-ex) orderings are often both present,

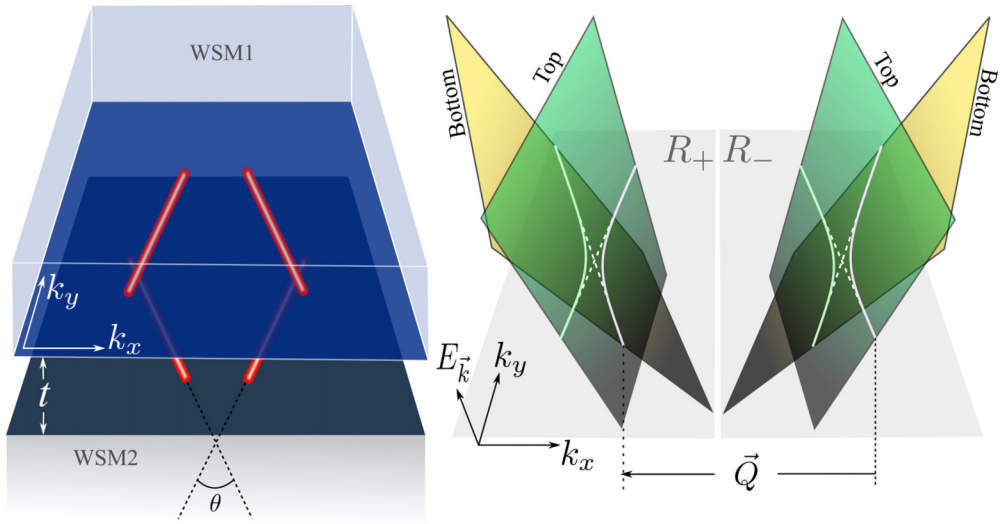

FIG. 1. Left: Two WSM surfaces with FAs indicated in the surface Brillouin zones, which are separated by a dielectric slab of thickness t. Two FAs reside on each surface with an angle θ between them. Right: Dispersions of the FAs. White dashed lines indicate Fermi surfaces without interactions. With interactions the Fermi surfaces distort to the solid white lines, allowing CDW and FFLO order to form with nesting vector $\vec{Q}$.

but tend to compete, so that as one type of ordering increases the other shrinks. With both present, the interlayer coherence should have spatial oscillations in real space. In addition to this, intralayer coherence between arcs on the same surface yields CDW order.

When CDW and exciton orders coexist, the system is in a supersolid state [45]. Such order has been considered for bilayer systems in which Wigner crystals may form at low electron density [46–48], and tends to be associated with excitons localizing at sites in a two-dimensional crystal. By contrast, in the coupled WSM surface system, the spatial ordering is determined by nesting vectors rather than by carrier density, so that there is no strong locking of the average interexciton separation with the CDW period. Thus, we expect the superfluid ordering to be more robust with respect to disorder than for the bilayer Wigner crystal system. A unique feature of the coupled FA system is the possibility of manipulating the relative strength of the spontaneous orderings by modifying the twist angle between surfaces, giving this system a level of tunability not present in more traditional materials. The presence of multiple continuously broken symmetries in this system implies that their superfluid modes will be coupled, so that counterflow superfluidity may become admixed with CDW sliding. This could yield threshold behavior in counterflow supercurrent, above which narrow band noise is sustained. Detection of such phenomenology associated with both exciton and CDW condensation would constitute direct evidence that the system hosts supersolid order.

II. MODEL

For concreteness, we consider a system of two WSMs with parallel surfaces labeled by an index $\eta = \pm 1$, a distance t apart, with each surface hosting two FAs labeled by an index $\xi = \pm 1$, in general not parallel to one another [Fig. 2(a)]. Each FA joins the projections of two Weyl nodes onto the surface Brillouin zone, with wave functions that decay exponentially in the bulk of the WSM. The associated decay length diverges at the Weyl node projections, which we model by the inverse of a mass function $M_\xi(\vec{k})$ [49]. The single-particle energy associated with each arc has the form $\epsilon_\xi(\vec{k}) = \pm\hbar v_F k_\perp^\xi$, which disperses with the momentum component perpendicular to the ark, $k_\perp^\xi$. Note the sign of this dispersion characterizes the helicity of the FA. Further details of the model are provided in the SM [44].

We model interactions among the electrons by

$$H_{\text{int}} = \sum_{\eta\eta'} \int_{\vec{r},\vec{r}'} V^{\eta\eta'}(\vec{r}-\vec{r}') : \hat{\rho}^{\eta}(\vec{r})\hat{\rho}^{\eta'}(\vec{r}') :, \qquad (1)$$

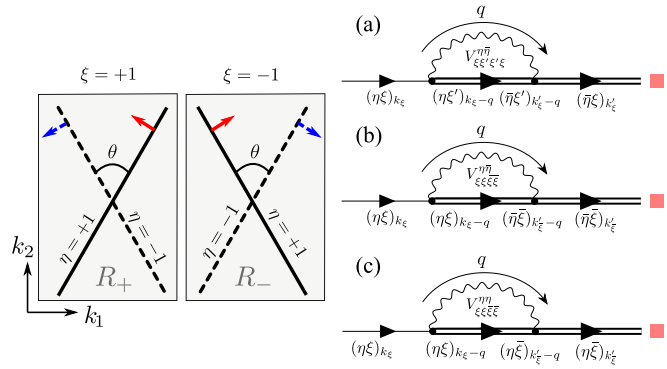

FIG. 2. Left: Configurations of the FAs where solid and dashed lines denote the states on the two surfaces ($\eta = \pm 1$). $\xi = \pm 1$ are two FAs on the same surface, at momentum region R_ξ. Directions of dispersions are marked by arrows. Pairs of FAs with $\xi\eta = \pm 1$ are nested with momentum $\vec{Q}$, which disperse in opposite directions. Right: Self-energy diagrams which describe spontaneously broken symmetries. k_ξ, q represent four vectors, with momenta $\vec{k}_\xi \in R_\xi$. (a), (b), and (c) gives rise to self-energies for D-ex, FFLO-ex, and CDW orders, respectively. ■ stands for any of (η, ξ).

where $\hat{\rho}^{\eta} = \sum_{\xi\xi'} \hat{\Psi}^{\eta\dagger}_{\xi} \hat{\Psi}^{\eta}_{\xi'}$, with $\hat{\Psi}^{\eta}_{\xi}$ being the field operator of the (η, ξ) FA. The functions $V^{++} = V^{--}$ and $V^{+-} = V^{-+}$ are the intra- and intersurface Coulomb interactions, respectively [44]. The decay depth of the single-particle states entering our decomposition of the field operators $\hat{\Psi}^{\eta}_{\xi}$ impacts the matrix elements appearing when Eq. (1) is written in terms of the noninteracting FA states; beyond this, our model is two-dimensional. We do not explicitly include bulk states in our analysis, although they can be approximately accounted for via screening in the interactions.

III. GREEN'S FUNCTION AND BROKEN SYMMETRY STATES

With these simplifications, components of the noninteracting finite-temperature Green's function of the WSM surfaces are given by $\mathcal{G}^{0}_{ij}(\vec{k}, i\omega_n) = \delta_{ij}/[i\omega_n - \epsilon_i(\vec{k})]$, where $\omega_n = (2n+1)/k_B T$ are the fermionic Matsubara frequencies at temperature T and the i, j subscripts are composite indices for η and ξ. To describe the broken symmetry states, we include interactions through a self-energy matrix Σ, which introduces components in the Green's function even for $i \neq j$, as well as between different wave vectors. These encode spontaneous ordering between different flavors of the fermions as well as possible translation symmetry breaking. We summarize the important diagrammatic terms that appear, within the noncrossing approximation [50,51], in Fig. 2(b).

In general, the full Green's function $\mathcal{G}$, noninteracting Green's function $\mathcal{G}^0$, and self-energy are related by the Dyson equation, to be solved self-consistently, $\mathcal{G} = \mathcal{G}^0 + \mathcal{G}^0 \Sigma \mathcal{G}$. The diagrams illustrated in Fig. 2(b) represent the last term in this equation. Numerical solution of these requires integration over momentum, which we approximate as a discrete sum over limited regions [denoted by R_ξ in Fig. 2(a)] of the surface Brillouin zone in the vicinities of the FAs. In addition, there is a Mastubara frequency sum, and the resulting self-energies are then independent of frequency because our model interaction is frequency independent. Further details of our numerical scheme are in the SM [44].

Denoting $\bar{\eta} = -\eta$ and $\bar{\xi} = -\xi$, and k_ξ for the three-momentum $(\vec{k}_\xi, \omega_n)$, we group the self-energies into three classes. Coherence between FAs on different surfaces that do not spontaneously break translation symmetry have the form $\Sigma^{\eta\bar{\eta}}_{\xi\bar{\xi}}(k_\xi, k'_{\bar{\xi}})$, and represent direct exciton order (D-ex) [23]. In addition, coherence between FAs on different surfaces which are separated in wave vector can also form, breaking both the gauge symmetry associated with individual layers and translational symmetry spontaneously, resulting in FFLO-ex order. Such ordering is encoded in self-energy terms of the form $\Sigma^{\eta\bar{\eta}}_{\xi\bar{\xi}}(k_\xi, k'_{\bar{\xi}})$. Finally, intralayer interactions also give rise to self-energies of the form $\Sigma^{\eta\eta}_{\xi\bar{\xi}}(k_\xi, k'_{\bar{\xi}})$, which indicate CDW order within a surface. For simplicity, we neglect the diagonal terms in the self-energy $\Sigma^{\eta\eta}_{\xi\xi}$, which are expected to simply renormalize the noninteracting FA velocities.

Before we discuss our numerical results, several comments are in order. Firstly, for the particular FA orientations shown in Fig. 1, some FAs have parallel sections with nesting momentum $\vec{Q}$. Particularly for the FFLO-ex order, one expects

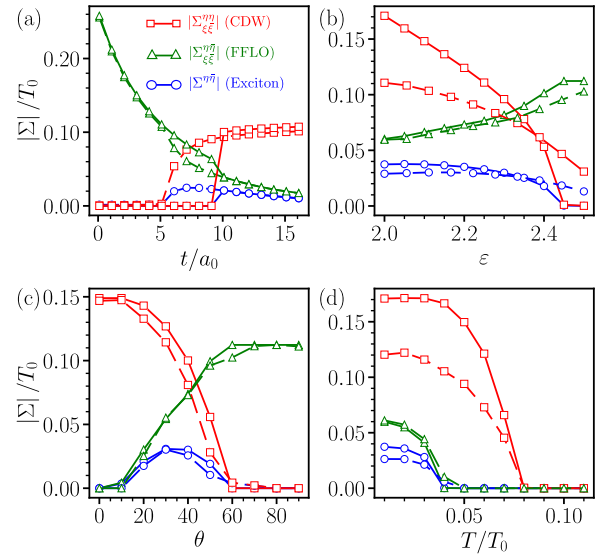

FIG. 3. Behavior of maximum order parameter magnitudes with system parameters. Variation with (a) surface separation (t), (b) WSM dielectric constant (ε), and (c) FA tilt angle (θ). Solid lines represent numerical results where the constraint Eq. (2) is enforced. Results marked by dashed lines have these constraints relaxed. (d) Critical temperatures of the three order parameters, in units of T_0 (see main text). $\theta = 60^\circ$ is used in (a), (b), and (d). Other parameters: for (a), $\varepsilon = 2$; for (b), $t/a_0 = 5$; for (c), $t/a_0 = 5$, $\varepsilon = 2.5$; for (d), $t/a_0 = 5$, $\varepsilon = 2$. The separation of the Weyl nodes, as well as the nesting vector $|\vec{Q}|$, is taken to be 0.4 Å^{-1}.

the dominant contribution of $\Sigma^{\eta\bar{\eta}}_{\xi\bar{\xi}}(\vec{k}_\xi, \vec{k}'_{\bar{\xi}})$ to occur at

$$\vec{k}_\xi - \vec{k}'_{\bar{\xi}} = \pm\vec{Q}. \tag{2}$$

Our numerical findings verify this for both FFLO-ex and CDW orders. Numerical calculations can be greatly simplified by assuming these self-energies vanish except at this momentum difference. We have compared this to results where the momentum difference is unconstrained in a few representative cases, and find rather good agreement [44]. Secondly, we characterize the strength of this Coulomb interaction by an effective fine-structure constant, $\alpha = (c/\varepsilon v_F)/137$. Unless otherwise specified, we assume $\alpha = 5/\varepsilon$, which is consistent with $v_F \sim 10^5$ m/s. For the intrasurface interaction we adopt a dielectric constant $\varepsilon = 4$, while for the intersurface interaction it is fixed at unity. We make the wave vectors and lengths unitless in terms of a lattice-spacing distance (a_0) and we consider the unit of our energy scale to be $T_0 = \hbar v_F/a_0$. With $a_0 \sim 5$ Å, we have T_0 of the order of 10^3 K.

IV. COMPETING PHASES

The numerical results we obtain indicate an intricate competition among the order parameters discussed above. Some typical results are illustrated in Fig. 3. At large t, for which interactions between surfaces are weak, intralayer CDW order dominates, while for smaller separation and stronger intersurface coupling, we find the FFLO-ex order dominates the CDW order. The competition between them is clearly visible in Figs. 3(a) and 3(b), in which we vary the separation between

layers, and hence the relative intra- and interlayer interactions. Interestingly, at small separation only the FFLO-ex order is present, but with increasing separation a transition occurs in which D-ex and CDW orders set in, accompanied by a sharp drop in the FFLO-ex order. This demonstrates the competition among the different types of order the system supports. Note that for much of the parameter regime, the simplifying assumption expressed in Eq. (2) yields results largely consistent with calculations where this constraint is relaxed, except in the transition region, where it is necessary to relax the constraint to correctly capture its second order nature.

For fixed separation, it is notable that increasing the tilt angle between the arcs tends to enhance the FFLO-ex order at the expense of the D-ex and CDW orders, as shown in Fig. 3(c). This is clearly a consequence of the strong nesting between the arcs involved in the FFLO-ex ordering, which persists at all angles. The relatively stronger stability of this ordering is also apparent in the temperature dependence of the order parameters, illustrated in Fig. 3(d), indicating different critical temperatures for FFLO-ex and CDW orders. Interestingly, we find that the critical temperature of the direct exciton order coincides with that of the intralayer CDW order. At low temperatures, all three orders may coexist, and with rising temperature a transition may take place from such a *multiply-ordered phase* to a phase with only FFLO-ex order. This intricate interplay of competition and cooperation among the different possible broken symmetries is one of the central results of this work.

Note that the FA dispersions shown in Fig. 2(a) are oriented so that nested FAs of opposite surfaces disperse in opposite directions. This supports the FFLO-ex order. One may also consider situations in which they disperse in the *same* direction. This could occur, for example, in WSMs with bulk magnetizations with opposite orientations. This results in the loss of FFLO-ex order. Introduction of curvature in the FAs also tends to suppress this order, although does not eliminate it (see SM [44].)

V. GOLDSTONE MODES AND COUNTERFLOW CURRENTS

Our model system involves four flavors of fermions (specified by η and ξ), and each has an individually conserved charge that is encoded by a $U(1)$ symmetry. The mean-field ground states we find spontaneously break at most three of these symmetries, so that all our phases respect global charge conservation. Although in general the six self-energy terms ($\Sigma^{\eta\eta'}_{\xi\xi'}$, excluding $\xi = \xi'$ and $\eta = \eta'$) may attain nonzero values, their phases $\theta^{\eta\eta'}_{\xi\xi'}$ are not independent. A close examination of the equations for the self-energies reveals the relations, $\theta^{+-}_{\xi\bar{\xi}} + \theta^{++}_{\bar{\xi}\xi} = n_1\pi$, $\theta^{+-}_{\xi\bar{\xi}} + \theta^{-+}_{\xi\bar{\xi}} = n_2\pi$, $\theta^{\eta\bar{\eta}}_{-+} + \theta^{\eta\eta}_{+-} = n_3\pi$, where repeated indices are summed and the n_i's may be 0 or ± 1 depending on the parameters. Fluctuations of the phases that violate the above relations are massive, but variations which keep these relations intact increase the energy of the system only when they have spatial or temporal gradients. Thus, we expect our system to support three gapless Goldstone modes. As detailed in the SM [44], one may formally derive an effective action for phase fluctuations valid for small gradients in terms of three independent phases, θ_i ($i = 1, 2, 3$), $S[\{\theta_i\}] \approx \sum_q \sum_{m,n} \Pi_{mn}(q)\theta_n(q)\theta_m(-q)$, where $\Pi_{nm}(q)$ is the polarizability function. The normal modes of S represent gapless modes $\tilde{\theta}_i$ which are linear combinations of θ_i. Static spatial gradients in these phases generally represent supercurrents, $(j^{\eta}_{\xi})_l = \sum_{i=1,2,3} \Gamma^{l}_{\eta\xi i} \nabla_l \tilde{\theta}_i$. We present details of the form of Γ for a simplified model in the SM [44]; in general, it depends on details of the system parameters and broken symmetries encoded in the Σ matrix. The entangling of different types of supercurrents, usually associated with interlayer counterflow currents [39] or sliding CDW modes [33], is an important signature that in the generic case the ground state of this system is a *supersolid.* Remarkably, for inversion-symmetric cases, we find a sum rule, $\sum_{\xi\eta}(j^{\eta}_{\xi})_l = 0$, indicating that the system does not support charged supercurrents. While natural for particle-hole condensates, which support counterflow supercurrents, this is less obvious for CDW dynamics which support sliding modes. We discuss the implications of this below.

VI. DISCUSSION AND SUMMARY

We have demonstrated that parallel surfaces of WSMs, with each hosting multiple FAs, in general support broken symmetries within and between the surfaces. In particular, we show that FFLO-exciton order may completely suppress direct-exciton and CDW orders, or may coexist with them. In the latter case the system is a supersolid. The entangling of orders in such a system is evidenced by its Goldstone modes, which in general have mixed counterflow—sliding CDW characters. In real systems, sliding behavior of CDWs are not observed as a dissipationless current, because their broken translational symmetry necessarily implies they will become pinned by disorder. Nevertheless, they host unique transport signatures: threshold driving fields above which a CDW may depin, and narrow-band noise with frequency proportional to the current above threshold [33]. An interesting signature of the supersolid character of this system would be the observation of these signatures in a counterflow experiment.

Several materials represent potential candidates for the physics described in this study. These include spinel compounds (such as VMg_2O_4) [52] and cobalt-based semimetals (such as $Co_3Sn_2S_2$). The former has two FAs on (110) surfaces, which are noncolinear and may serve as potential hosts for the physics we describe. For certain surface terminations, $Co_3Sn_2S_2$ has three FAs which are oriented at 120° angle with each other. For two such surfaces oriented at $\sim$180°, one will have four FAs in approximately the configuration we consider; the other two may support their own FFLO-exciton condensation, but will essentially decouple from the other four FAs (see SM [44]).

For simplification of the numerical analysis, we considered straight FAs for the noninteracting WSM surfaces. As argued in Ref. [29], in the presence of a curvature in the FAs, there is an associated first-order phase transition with increasing curvature of the FAs. A full solution for the interacting Green's function in this case is numerically challenging; some results are presented in the SM [44]. Moreover, in our idealization of these systems we have ignored the presence of bulk states

which may be present at the Fermi energy, and can have finite support at the surfaces. Their impact on the broken symmetry states and associated supercurrents are interesting subjects for further study of these remarkably rich systems.

ACKNOWLEDGMENTS

A.K. acknowledges support from the SERB (Government of India) via Sanction No. ECR/2018/001443, DAE (Government of India) via Sanction No. 58/20/15/2019-BRNS, as well as MHRD (Government of India) via Sanction No. SPARC/2018-2019/P538/SL. H.A.F. acknowledges support from the NSF via Grants No. ECCS-1936406 and No. DMR-1914451, as well as the support of the Research Corporation for Science Advancement through a Cottrell SEED Award, and the US-Israel Binational Science Foundation through Award No. 2016130. We also acknowledge the use of the HPC facility at IIT Kanpur. A.K. also acknowledges support from MHRD (Government of India) through SPARC initiative via Sanction No. SPARC/2018-2019/7/SL(IN).

[1] N. P. Armitage, E. J. Mele, and A. Vishwanath, Rev. Mod. Phys. **90**, 015001 (2018); S. Jia, S.-Y. Xu, and M. Z. Hasan, Nat. Mater. **15**, 1140 (2016); S. Rao, J. Indian Inst. Sci. **96**, 2 (2016).
[2] E. V. Gorbar, V. A. Miransky, I. A. Shovkovy, and P. O. Sukhachov, *Electronic Properties of Dirac and Weyl Semimetals* (World Scientific, Singapore, 2021).
[3] B. Q. Lv, H. M. Weng, B. B. Fu, X. P. Wang, H. Miao, J. Ma, P. Richard, X. C. Huang, L. X. Zhao, G. F. Chen, Z. Fang, X. Dai, T. Qian, and H. Ding, Phys. Rev. X **5**, 031013 (2015).
[4] C. Zhang, Z. Ni, J. Zhang, X. Yuan, Y. Liu, Y. Zou, Z. Liao, Y. Du, A. Narayan, H. Zhang, T. Gu, X. Zhu, L. Pi, S. Sanvito, X. Han, J. Zou, Y. Shi, X. Wan, S. Y. Savrasov, and F. Xiu, Nat. Mater. **18**, 482 (2019).
[5] Z. Rao, H. Li, T. Zhang, S. Tian, C. Li, B. Fu, C. Tang, L. Wang, Z. Li, W. Fan, J. Li, Y. Huang, Z. Liu, Y. Long, C. Fang, H. Weng, Y. Shi, H. Lei, Y. Sun, T. Qian *et al.*, Nature (London) **567**, 496 (2019).
[6] G. Li, Q. Xu, W. Shi, C. Fu, L. Jiao, M. E. Kamminga, M. Yu, H. Tüysüz, N. Kumar, V. Süß, R. Saha, A. K. Srivastava, S. Wirth, G. Auffermann, J. Gooth, S. Parkin, Y. Sun, E. Liu, and C. Felser, Sci. Adv. **5**, eaaw9867 (2019).
[7] M. Tanaka, Y. Fujishiro, M. Mogi, Y. Kaneko, T. Yokosawa, N. Kanazawa, S. Minami, T. Koretsune, R. Arita, S. Tarucha, M. Yamamoto, and Y. Tokura, Nano Lett. **20**, 7476 (2020).
[8] H. Yi, Z. Wang, C. Chen, Y. Shi, Y. Feng, A. Liang, Z. Xie, S. He, J. He, Y. Peng, X. Liu, Y. Liu, L. Zhao, G. Liu, X. Dong, J. Zhang, M. Nakatake, M. Arita, K. Shimada, H. Namatame *et al.*, Sci. Rep. **4**, 6106 (2014).
[9] S.-Y. Xu, N. Alidoust, I. Belopolski, Z. Yuan, G. Bian, T.-R. Chang, H. Zheng, V. N. Strocov, D. S. Sanchez, G. Chang, C. Zhang, D. Mou, Y. Wu, L. Huang, C.-C. Lee, S.-M. Huang, BaoKai Wang, A. Bansil, H.-T. Jeng, T. Neupert, A. Kaminski *et al.*, Nat. Phys. **11**, 748 (2015).
[10] M. Kargarian, M. Randeria, and Y.-M. Lu, Proc. Natl. Acad. Sci. USA **113**, 8648 (2016).
[11] P. J. W. Moll, N. L. Nair, T. Helm, A. C. Potter, I. Kimchi, A. Vishwanath, and J. G. Analytis, Nature (London) **535**, 266 (2016).
[12] Y. Wu, N. H. Jo, L.-L. Wang, C. A. Schmidt, K. M. Neilson, B. Schrunk, P. Swatek, A. Eaton, S. L. Bud'ko, P. C. Canfield, and A. Kaminski, Phys. Rev. B **99**, 161113(R) (2019).
[13] C.-Z. Li, A.-Q. Wang, C. Li, W.-Z. Zheng, A. Brinkman, D.-P. Yu, and Z.-M. Liao, Nat. Commun. **11**, 1150 (2020).
[14] J. Hofmann and S. Das Sarma, Phys. Rev. B **93**, 241402(R) (2016).
[15] G. M. Andolina, F. M. D. Pellegrino, F. H. L. Koppens, and M. Polini, Phys. Rev. B **97**, 125431 (2018).
[16] G. Chiarello, J. Hofmann, Z. Li, V. Fabio, L. Guo, X. Chen, S. Das Sarma, and A. Politano, Phys. Rev. B **99**, 121401(R) (2019).
[17] E. V. Gorbar, V. A. Miransky, I. A. Shovkovy, and P. O. Sukhachov, Phys. Rev. B **99**, 155120 (2019).
[18] K. Tsuchikawa, S. Konabe, T. Yamamoto, and S. Kawabata, Phys. Rev. B **102**, 035443 (2020).
[19] J. C. W. Song and M. S. Rudner, Phys. Rev. B **96**, 205443 (2017).
[20] Ž. Bonačić Lošić, J. Phys.: Condens. Matter **30**, 365003 (2018).
[21] T. Tamaya, T. Kato, S. Konabe, and S. Kawabata, J. Phys.: Condens. Matter **31**, 305001 (2019).
[22] S. O. Abdol, A. S. Vala, and B. Abdollahipour, J. Phys.: Condens. Matter **31**, 335002 (2019).
[23] S. Ghosh and C. Timm, Phys. Rev. B **101**, 165402 (2020).
[24] H. Wei, S.-P. Chao, and V. Aji, Phys. Rev. Lett. **109**, 196403 (2012).
[25] M. Laubach, C. Platt, R. Thomale, T. Neupert, and S. Rachel, Phys. Rev. B **94**, 241102(R) (2016).
[26] V. Dwivedi, Phys. Rev. B **97**, 064201 (2018).
[27] G. Murthy, H. A. Fertig, and E. Shimshoni, Phys. Rev. Res. **2**, 013367 (2020).
[28] F. Abdulla, S. Rao, and G. Murthy, Phys. Rev. B **103**, 235308 (2021).
[29] P. Michetti and C. Timm, Phys. Rev. B **95**, 125435 (2017).
[30] C.-H. Zhang and Y. N. Joglekar, Phys. Rev. B **77**, 233405 (2008).
[31] M. Yu. Kharitonov and K. B. Efetov, Phys. Rev. B **78**, 241401(R) (2008).
[32] D. S. L. Abergel, R. Sensarma, and S. Das Sarma, Phys. Rev. B **86**, 161412(R) (2012).
[33] G. Grüner, Rev. Mod. Phys. **60**, 1129 (1988).
[34] D. Snoke, Science **298**, 1368 (2002).
[35] H. Min, R. Bistritzer, J.-J. Su, and A. H. MacDonald, Phys. Rev. B **78**, 121401(R) (2008).
[36] M. M. Fogler, L. V. Butov, and K. S. Novoselov, Nat. Commun. **5**, 4555 (2014).
[37] M. Combescot, R. Combescot, and F. Dubin, Rep. Prog. Phys. **80**, 066501 (2017).
[38] F. Dolcini, D. Rainis, F. Taddei, M. Polini, R. Fazio, and A. H. MacDonald, Phys. Rev. Lett. **104**, 027004 (2010).
[39] J. Eisenstein, Annu. Rev. Condens. Matter Phys. **5**, 159 (2014).
[40] J.-J. Su and A. H. MacDonald, Nat. Phys. **4**, 799 (2008).
[41] A. V. Balatsky, Y. N. Joglekar, and P. B. Littlewood, Phys. Rev. Lett. **93**, 266801 (2004).
[42] M. P. Mink, H. T. C. Stoof, R. A. Duine, M. Polini, and G. Vignale, Phys. Rev. Lett. **108**, 186402 (2012).

[43] J. A. Seamons, C. P. Morath, J. L. Reno, and M. P. Lilly, Phys. Rev. Lett. **102**, 026804 (2009).

[44] See Supplemental Material at http://link.aps.org/supplemental/10.1103/PhysRevB.107.L041402, where we discuss (i) theoretical details of the dispersions of multiple Fermi arcs (FA) that we consider, (ii) Coulomb matrix elements, scattering vertices, and the construction of self-energies for solving the interacting Green's function, (iii) variation of the self-energy amplitudes with system parameters, (iv) action of phase fluctuations and the condition of counterflow currents on the FAs, and (v) the case of the three-FA system.

[45] M. Boninsegni and N. V. Prokof'ev, Rev. Mod. Phys. **84**, 759 (2012).

[46] Y. N. Joglekar, A. V. Balatsky, and S. Das Sarma, Phys. Rev. B **74**, 233302 (2006).

[47] L. Zheng and H. A. Fertig, Phys. Rev. B **52**, 12282 (1995).

[48] S. Narasimhan and T.-L. Ho, Phys. Rev. B **52**, 12291 (1995).

[49] S. Verma, D. Giri, H. A. Fertig, and A. Kundu, Phys. Rev. B **101**, 085419 (2020).

[50] A. Altland and B. Simons, *Condensed Matter Field Theory*, 2nd ed. (Cambridge University Press, Cambridge, 2010).

[51] G. Giuliani and G. Vignale, *Quantum Theory of the Electron Liquid* (Cambridge University Press, Cambridge, 2005).

[52] W. Jiang, H. Huang, F. Liu, J.-P. Wang, and T. Low, Phys. Rev. B **101**, 121113(R) (2020).